Letter

Andreev processes in mesoscopic multiterminal graphene Josephson junctions

Fan Zhang, Asmaul Smitha Rashid, Mostafa Tanhayi Ahari, Wei Zhang, Krishnan Mekkanamkulam Ananthanarayanan, Run Xiao, George J. de Coster, 4 Matthew J. Gilbert, 3,5 Nitin Samarth, 1,* and Morteza Kayyalha 2,†

¹Department of Physics, The Pennsylvania State University, University Park, Pennsylvania 16802, USA 2 Department of Electrical Engineering, The Pennsylvania State University, University Park, Pennsylvania 16802, USA ³Materials Research Laboratory, The Grainger College of Engineering, University of Illinois, Urbana-Champaign, Illinois 61801, USA ⁴DEVCOM Army Research Laboratory, 2800 Powder Mill Rd, Adelphi, Maryland 20783, USA ⁵Department of Electrical Engineering, University of Illinois, Urbana-Champaign, Illinois 61801, USA



(Received 12 October 2022; revised 27 March 2023; accepted 28 March 2023; published 12 April 2023)

There is growing interest in using multiterminal Josephson junctions (MTJJs) as a platform to artificially emulate topological phases and to investigate superconducting mechanisms such as multiplet Cooper pairings. Current experimental signatures in MTJJs have led to conflicting interpretations of the salient features. In this work, we report a collaborative experimental and theoretical investigation of graphene-based four-terminal Josephson junctions. We observe resonant features in the differential resistance maps that resemble those ascribed to multiplet Cooper pairings. To understand these features, we model our junctions using a circuit network of resistively and capacitively shunted junctions (RCSJs). We find that the RCSJ model successfully reproduces the observed multiplet features. Therefore, our study suggests that differential resistance measurements alone are insufficient to conclusively distinguish resonant Andreev reflection processes from semiclassical circuit-network effects.

DOI: 10.1103/PhysRevB.107.L140503

The Josephson effect is a centerpiece of many quantum device applications, including superconducting quantum interference devices (SQUIDs) and superconducting qubits [1,2]. Increasing the number of superconducting terminals beyond the typical two terminals in Josephson junctions (JJs) leads to nonlocal coupling of superconducting order parameters through a common scattering region. This nonlocal coupling has been predicted to lead to quartet Cooper pairings [3] and macroscopic multichannel effects such as voltage-induced Shapiro steps, phase drag, and magnetic flux transfer [4-7]. More recently, multiterminal Josephson junctions (MTJJs) have been proposed as a platform to emulate topological phases in artificial dimensions [8-21]. In MTJJs with n superconducting terminals, the energy of the Andreev bound states is a function of (n-1) independent phases. In this context, the phase differences between superconducting terminals are treated as quasimomenta of a crystal forming a Brillouin zone in (n-1) dimensions. The resultant band structure is predicted to display topological properties such as Weyl singularities [10,11]. While providing strong motivation for studying the multiterminal Josephson effect, the exploration of MTJJs as a platform for engineering artificial topological systems is still nascent.

MTJJs have been experimentally explored in various materials platforms including graphene/MoRe [22,23], graphene/Al [24], and InAs/Al [25-29]. These experiments

focused on the gate and magnetic field dependence of the supercurrent flow between adjacent and nonadjacent superconducting terminals [27]. Additionally, these experiments studied the nontrivial geometric response of the critical current contour (CCC), a generic characteristic defining the region in which all the superconducting terminals are at zero voltage [26]. Recent studies have also reported signatures of quartet pairings [24,25,30], arising from crossed Andreev reflection processes. However, studies of three-terminal Josephson junctions [23] and a network of tunnel junctions [31] argue that the multiplet features may also arise from circuit-network effects.

In this paper, we use a coordinated experimental and theoretical approach to critically understand the currentvoltage characteristics of four-terminal JJs fabricated in hBN-encapsulated graphene heterostructures. We model our junctions using a circuit network of coupled resistively and capacitively shunted junctions (RCSJs). We show that the semiclassical RCSJ model reproduces the observed multiplet features, which are similar in nature to those predicted for multiplet Cooper pairings [24,25,30]. To elucidate the underlying mechanisms giving rise to these features, we calculate the contribution of the quasiparticle current which reveals the pair current contribution to the total current. We further consider materials-specific properties such as the Fermi surface geometry of the normal material and junction transparency by incorporating the relevant current-phase relation (CPR) into the RCSJ model. We find theoretically that the shape of the CCC depends on the specific form of the CPR [26]. Finally, our study demonstrates that circuit-network effects,

^{*}Corresponding author: nsamarth@psu.edu

[†]Corresponding author: mzk463@psu.edu

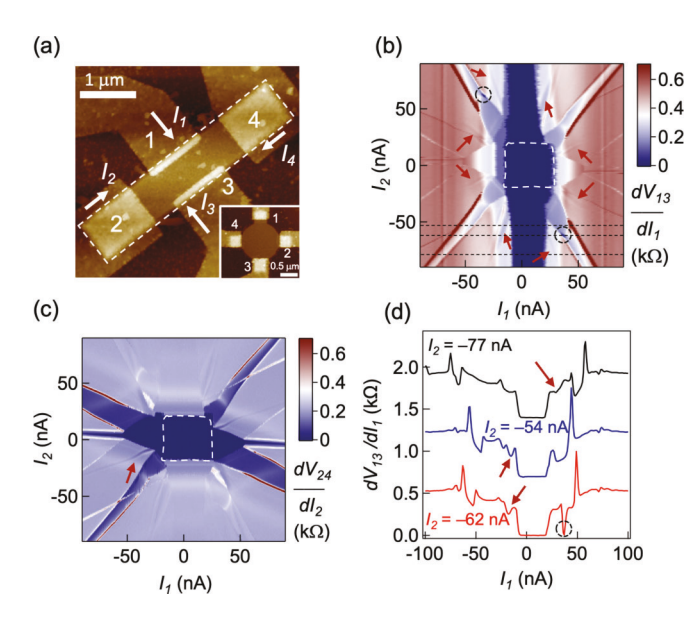


FIG. 1. (a) The atomic force microscope (AFM) image of device A. Inset shows the AFM image of device B. The Josephson junctions are made of hBN-graphene-hBN (outlined by white dashed line) edge contacted with superconducting Al terminals. Arrows show the directions of bias currents. (b) and (c) Color map of the differential resistance dV_{13}/dI_1 (b), and dV_{24}/dI_2 (c) versus $I_1=-I_3$ and $I_2=-I_4$ of device A at $V_g=50$ V and T=12 mK. The differential resistances are measured using lock-in amplifiers. Arrows and black circles mark resonant branches along local minima of dV_{13}/dI_1 and near-zero differential resistance, respectively. Dashed white contours outline the critical current contour corresponding to V=0 V for all superconducting terminals. (d) dV_{13}/dI_1 vs I_1 along horizontal black dashed lines in panel (b). The local minima and near-zero differential resistance are marked with arrows and circles as in (b). Curves are shifted vertically by 0.7 k Ω for clarity.

predicted by the RCSJ model, lead to macroscopic signatures in differential resistance maps that are identical to those ascribed to multiplet pairings.

The results presented in the main text are based on two devices: device A and B [Fig. 1(a)]. The channel length of device A is 0.8 μ m and 3 μ m along current I_{13} and I_{24} directions, respectively. Device B has a circular geometry with a diameter of 1.3 μ m. We mark the current directions used for the transport measurements in Fig. 1(a). We set $I_1 = -I_3$ and $I_2 = -I_4$ in our experiments. We perform all of the measurements using a lock-in amplifier technique with an excitation current of 1 nA at T = 12 mK, if not otherwise specified.

Figures 1(b) and 1(c) plot differential resistances dV_{13}/dI_1 and dV_{24}/dI_2 versus I_1 and I_2 at $V_g = 50$ V, respectively. The critical current contour (CCC) is indicated with white dashed contours on these maps. Consistent with previous reports in MTJJs [22–29], we observe differential resistance minima corresponding to the superconducting coupling between the terminal pairs as well as multiple Andreev reflections (MARs). These features are discussed in more details in the Supplemental Material [32] (see also Refs. [33–36] therein). In the remainder of this Letter, we focus primarily on the local minima in differential resistance maps that are attributed to the multiplet pairings [red arrows in Figs. 1(b) and 1(c)]. To

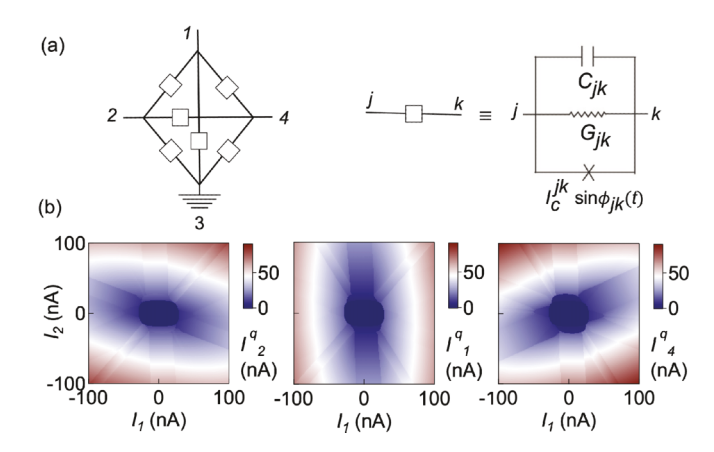


FIG. 2. (a) Schematic of the circuit-network of coupled RCSJs utilized to simulate a four-terminal JJ in which the third terminal is grounded. The links between terminals, e.g., j and k, are characterized by the sinusoidal CPR $I_c^{jk} \sin \phi_{jk}(t)$, a shunted conductance G_{jk} , and capacitance C_{jk} . (b) Calculated quasiparticle current I_j^q as a function of the input currents obtained from the coupled RCSJ model. The boundary of the region where $I_j^q = 0$ determines the CCC.

better highlight these minima, Fig. 1(d) depicts cuts along the dashed horizontal lines in Fig. 1(b).

To elucidate the underlying origin of the observed multiplet features, we consider a circuit-network model of coupled RCSJs [Fig. 2(a)]. The RCSJ model represents the individual junctions by a two-fluid system in which the total junction current is the sum of a dissipative quasiparticle current $i_{ik}^q(t)$ and a pair current $i_{jk}^p(t)$ [37]. The quasiparticle current is due to a finite voltage $V_{jk}(t)$ across the junction that exceeds the superconducting gap, $i_{jk}^q(t) = G_{jk}V_{jk}(t)$, where G_{jk} is a constant phenomenological conductance tensor. The pair current is given by the diffusive CPR $i_{jk}^p(t) = I_c^{jk} \sin(\phi_{jk}(t))$, where I_c^{jk} is the critical current and $\phi_{ik}(t) \equiv \phi_i(t) - \phi_k(t)$ is the gauge-invariant phase difference satisfying the Josephson equation $d\phi_{ik}(t)/dt = (2e/\hbar)V_{ik}(t)$. Here, we assume a diffusive CPR for the junctions. However, we note that the CPR for ballistic, diffusive, or φ_0 junctions do not change our overall conclusions. Subsequently, we assume that the junctions are characterized by the presence of a shunt capacitance C_{ik} , which is the characteristic of circuits involving Josephson junctions in a wide family of weak links [38]. For the numerical analysis that follows below, we start by choosing experimentally relevant values for the modeling parameters (e.g., resistance and critical current). We then fine tune the parameters through inspection to numerically obtain differential resistance maps which are similar to the experimental ones. Imposing current conservation (Kirchhoff's current law) at the terminal *j* yields

$$I_{j} = \sum_{k} \left(i_{jk}^{p} + i_{jk}^{q} + C_{jk} \frac{dV_{jk}(t)}{dt} \right). \tag{1}$$

Equation (1) results in three coupled differential equations that may be solved for the relevant junction phases $(\phi_2(t), \phi_1(t), \phi_4(t))$, assuming that one of the terminals is grounded, i.e., $\phi_3(t) = 0$ as shown in Fig. 2(a). The d.c.

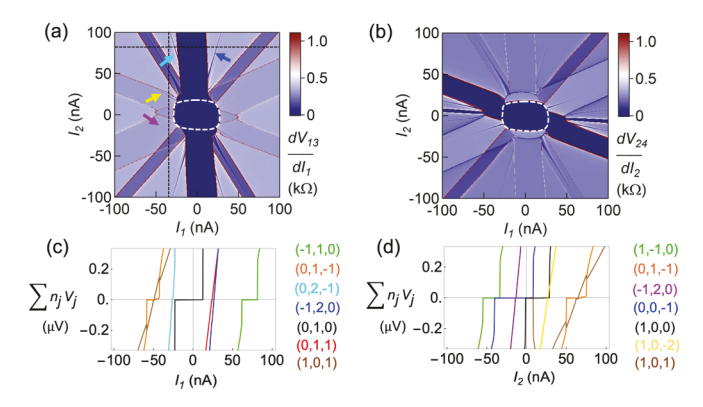


FIG. 3. Theoretical simulation of differential resistance dV_{13}/dI_1 (a), and dV_{24}/dI_2 (b) versus I_1 and $I_2 = -I_4$ obtained from the coupled RCSJ model. The white dashed contours show the CCC, which encloses the region in which $I^q = 0$. (c) $\sum_j n_j V_j$ as a function of I_1 for a line cut at $I_2 = 80$ nA, along the horizontal dashed line in panel (a). (d) $\sum_j n_j V_j$ as a function of I_2 for a line cut at $I_1 = -40$ nA, along the vertical dashed line in panel (a). Each branch that is crossed by the black dashed line in panel (a) corresponds to a unique triplet (n_2, n_1, n_4) satisfying $\sum_j n_j V_j = 0$. Only the narrow branches, indicated with the small arrows, correspond to higher-order harmonics.

voltages, relative to the grounded terminal, are obtained by taking the time average as $\langle V_{j3}(t)\rangle = (\hbar/2e)\langle d\phi_j(t)/dt\rangle \equiv V_i$.

To separate out the contributions of quasiparticle and pair currents to the total current flowing between different terminal pairs, we take the time average of Eq. (1). We note that any nonzero voltage between terminals j and k results in a nonzero quasiparticle current: $I_{jk}^q \equiv G_{jk}(V_j - V_k)$. We define the CCC as the region wherein the current is solely carried by the pair contribution and, accordingly, the quasiparticle contribution is zero. Figure 2(b) shows $I_j^q \equiv \left(\sum_k (I_{jk}^q)^2\right)^{1/2}$ as a function of the input currents. In the central region, the dark blue area in Fig. 2(b), $I_i^q = 0$ and all the terminals are at zero voltage.

Figure 3 depicts the calculated differential resistance $d(V_j - V_k)/dI_j \equiv dV_{jk}/dI_j$ as a function of the input currents, I_1 and I_2 . We observe that the RCSJ model successfully reproduces all the major branches including those marked by arrows in Fig. 1(b). However, as expected, it does not capture the phase-coherent processes such as multiple Andreev Reflections (MARs) (see the Supplemental Material [32] for more details). We further note that the multiplet branches [marked by arrows in Fig. 3(a)] in the dV/dI maps exhibit a radial inversion symmetry. These branches can be identified by a unique triplet (n_2, n_1, n_4) satisfying

$$\sum_{i} n_j V_j = 0, \tag{2}$$

where n_2 , n_1 , and n_4 are integers. Figures 3(c) and 3(d) highlight such triplets for branches crossing the black dashed lines in Fig. 3(a).

To provide an analytical picture for our four-terminal JJ, we consider all the terminals are at zero voltage and $I_4 = 0$. We note that these assumptions are made to simplify the following analytical derivations and will not affect our overall conclu-

sions (see Supplemental Material [32] for more details). The energy F of the system is given by

$$F = -\frac{\hbar}{2e} \left(I_1 \phi_1 + I_2 \phi_2 + \sum_{i < k} I_c^{jk} \cos \phi_{jk} \right), \quad \phi_3 = 0. \quad (3)$$

We obtain ϕ_4 by minimizing F with respect to ϕ_4 for fixed (ϕ_2, ϕ_1) as

$$\phi_4 = \arctan \frac{\sum_{k \neq 4} I_c^{4k} \sin \phi_k}{\sum_{k \neq 4} I_c^{4k} \cos \phi_k}, \quad \phi_3 = 0.$$
 (4)

We can express the current flowing from terminal 4 to ground as

$$i_{43}^p = I_c^{43} \sin \phi_4. (5)$$

Generically, since ϕ_4 is a 2π -periodic odd function of (ϕ_2, ϕ_1) , i_{43}^p can be expanded as a Fourier series [31]:

$$i_{43}^p = \sum_{n_2, n_1} I_{n_2, n_1} \sin(n_2 \phi_2 + n_1 \phi_1),$$
 (6)

where (n_2, n_1) are integers and I_{n_2,n_1} is the amplitude of the (n_2, n_1) harmonic. We note that in a general case of $I_4 \neq 0$, a triplet (n_2, n_1, n_4) may emerge [see Figs. 3(c) and 3(d)].

According to Eq. (6), a dc pair current flows if I_{n_2,n_1} is non-zero and $n_2\phi_2 + n_1\phi_1$ is constant [31,39]. Inside the CCC, the pair current is non-zero because the phases are time-independent, leading to a zero voltage on each terminal $(V \propto d\phi/dt)$. We note that outside of the CCC, voltages are nonzero and Eq. (3) is no longer valid. However, in a nonequilibrium case in which both quasiparticle and pair currents may flow, one may utilize the nonequilibrium Green's functions method [40] to recover an analogous CPR to Eq. (6). Our numerical analysis suggests that outside CCC, a pair current may still emerge on the resonant branches where pairwise combinations of (n_2, n_1) satisfies $n_2\phi_2(t) + n_1\phi_1(t) = \text{const.}$

We point out that starting from a semiclassical RCSJ model, in which terminals are pairwise coupled, the circuitnetwork model may result in a nonlocal transfer of Cooper pairs between two terminals. For example, Eq. (6) suggests that n_1 and n_2 Cooper pairs are respectively transferred from ground to terminals 1 and 2 through terminal 4 [41]. Therefore, it is challenging to separate nonlocal phase-coherent Andreev reflection processes from the semiclassical circuitnetwork effects as both processes may result in similar macroscopic transport observables. More sophisticated measurements, such as correlated noise spectroscopy [25,42], provide additional information required to distinguish these processes. We finally note that the RCSJ model does not reproduce the near-zero differential resistance, marked by black dashed circles in Figs. 1(b) and 1(d), that re-emerges at a nonzero voltage bias (see the Supplemental Material [32] for more details). Understanding the origin of this phenomenon is a subject of future studies.

We now focus on device B, wherein the graphene region has a symmetric circular shape with a diameter of \sim 1.3 µm as shown in the inset of Fig. 1(a). Figures 4(a)–4(c) show the dV_{13}/dI_1 maps versus I_1 and I_2 at three different gate voltages $V_g = 20$ V, 40 V, and 60 V, respectively. Figure 4(d) depicts the dV_{13}/dI_1 map calculated from the RCSJ model, where the

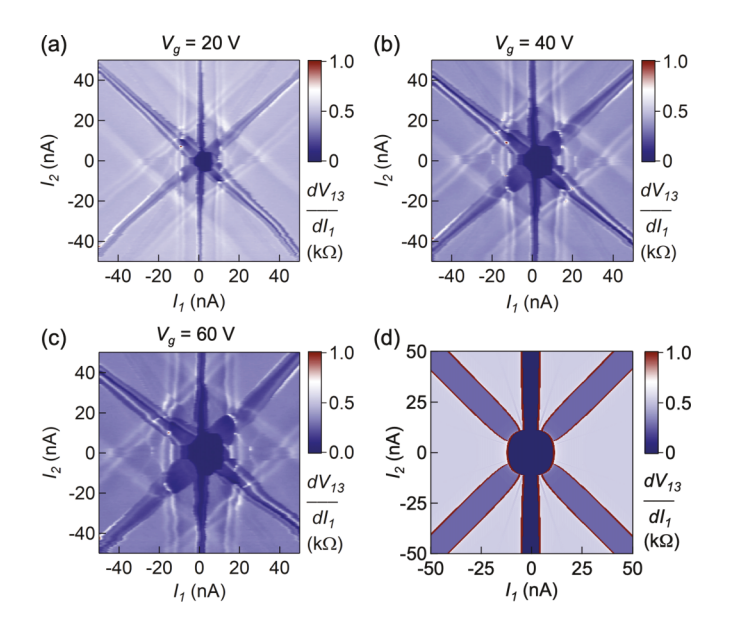


FIG. 4. (a)–(c) Color maps of the differential resistance (dV_{13}/dI_1) versus $I_1=-I_3$ and $I_2=-I_4$ of device B at three different gate voltages $V_g=20$ V (a), 40 V (b), and 60 V (c). The differential resistance is measured using a lock-in amplifier. All the measurements are performed at T=12 mK. (d) Theoretical simulation of the differential resistance (dV_{13}/dI_1) for a symmetric RCSJ configuration, i.e., $I_c^{jk}=5$ nA, and $G_{jk}=1/115$ Ω^{-1} .

same parameters are used for all the junctions. We observe that while the theoretical map captures the main features of the experimental data, it does not reproduce the repeating branches of local minima (see the Supplemental Material [32] for more details). Furthermore, we do not observe any signature of multiplet pairings [arrows in Fig. 1(b)] in our experimental results for device B even at $V_g = 60$ V. We note that the induced superconductivity is weaker in device B compared to device A, likely due to a lower contact transparency resulted from the fabrication process. This is supported by the fact that a lower critical current I_c is observed between terminals 2 and 4 in device B ($I_{c,B} \sim 10$ nA) at $V_g = 60$ V compared to device A ($I_{c,A} \sim 20$ nA) at $V_g = 50$ V. Moreover, we find that the multiplet branch in device A [red arrow in Fig. 1(c)] disappears at $V_g = -50$ V, where the induced superconductivity is weaker compared to $V_g = 50 \text{ V}$ (see the Supplemental Material [32] for more details). Finally, we observe that by decreasing V_g from 60 V to 20 V in the electron-doped regime (note the Dirac point is at $V_g = -11.25$ V), the area of the CCC monotonically decreases. In contrast to a previous report in InAs MTJJs [26], we observe that the gate only influences the size of the CCC; we do not see any obvious change in the geometry of the CCC (see the Supplemental Material [32] for the magnetic field dependence of the CCC in device A). This discrepancy may be related to the symmetric nature of the Fermi surface and lack of spin-orbit coupling in graphene compared to InAs. In general, the shape of the CCC in our devices is determined by an effective CPR which depends on the measurement configuration and current biases [43,44].

So far we have only considered diffusive transport in the RCSJ model. However, in graphene, it is important to consider ballistic limit to understand the evolution of the differen-

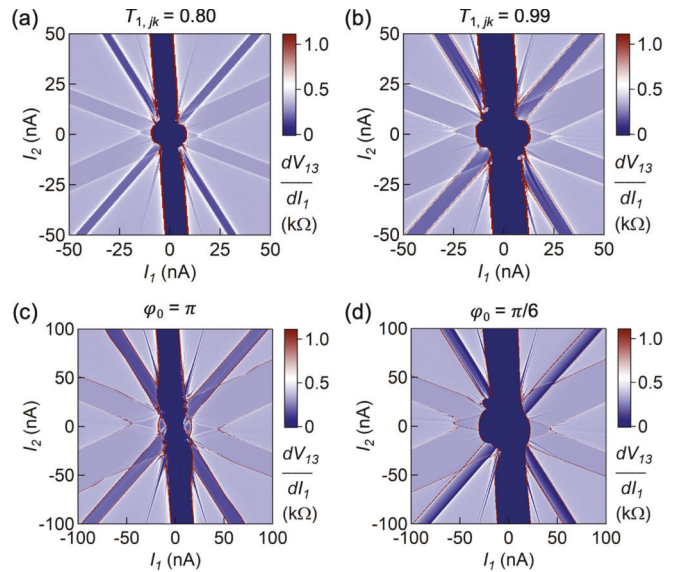


FIG. 5. (a) and (b) Theoretical simulation of differential resistance dV_{13}/dI_1 versus I_1 and $I_2=-I_4$ obtained from the coupled RCSJ model for a different junction transparency (a) $T_{1,jk}=0.80$, and (b) $T_{1,jk}=0.99$. (c) and (d) Theoretical simulation of differential resistance dV_{13}/dI_1 versus I_1 and $I_2=-I_4$ obtained from the coupled RCSJ model for φ_0 -junctions with a CPR between terminals j and k as $i_{jk}^p = I_c^{jk} \sin(\phi_{jk} - \varphi_0)$. Panel (c) is for $\varphi_0 = \pi$, and (d) is for $\varphi_0 = \pi/6$.

tial resistance and resonant features. Here, we consider that transport is mainly facilitated by the Andreev bound states localized in the junction region. As a result, the energy of the Andreev bound states for the junction between terminals j and k is given by $\varepsilon_{n,jk} = \Delta \sqrt{1 - T_{n,jk} \sin^2(\phi_{jk}/2)}$, where $T_{n,jk}$ is the transmission eigenvalue of the transport channel n. This results in the following CPR:

$$I_{jk} = -\frac{2e}{\hbar} \sum_{n} \frac{d\varepsilon_{n,jk}}{d\phi_j}.$$
 (7)

We note that with a strong elastic scattering at the junction region, i.e., $T_{n,jk} \ll 1$, the sinusoidal CPR can be recovered. Therefore, we only focus on the clean regime $T_{n,ik} \sim 1$ where the CPR deviates from the usual sinusoidal profile by developing a skewness. Figures 5(a) and 5(b) show the simulated differential resistance dV_{13}/dI_1 versus I_1 and I_2 for $T_{1,jk}$ = 0.8 and $T_{1,jk} = 0.99$, respectively. We observe that the differential resistance maps are qualitatively similar to the one shown in Fig. 3(a). This indicates that in the RCSJ model, the multiplet features are robust to the variation of the junction transparency. However, we experimentally observe that contact transparency may play a role in the observation of the multiplet signatures (see Fig. 4 and the Supplemental Material [32]). We note that a reduced contact transparency, e.g., due to an insulating barrier between graphene and aluminum, may result in an increased capacitance, which, in turn, may affect the width of the multiplet branches in the differential resistance maps obtained from the RCSJ model [23]. This is seen in our theoretical results in Fig. 4(d), where multiplet signatures are less visible because of the large capacitance values in the RCSJ model (see Table 2 in the Supplemental Material [32] for more details).

To better understand the impact of the CPR on the resonant features, we also consider a junction with Rashba spin-orbit coupling and magnetic order in the normal region. In this case, the CPR may take a sinusoidal form with a phase offset, $\sin(\phi-\varphi_0)$ [45]. We incorporate this modified CPR into our RCSJ model as $i_{jk}^p = I_c^{jk}\sin(\phi_{jk}-\varphi_0)$. Figures 5(c) and 5(d) show the differential resistance dV_{13}/dI_1 maps versus I_1 and $I_2=-I_4$ obtained from this RCSJ model for $\varphi_0=\pi$ and $\pi/6$, respectively. We observe that the CCC is significantly modified by φ_0 , whereas the resonant features outside of the CCC remain mainly independent of φ_0 and are qualitatively similar to those in Fig. 3(a). We note that in general, the phase shift φ_0 may originate from various microscopic mechanisms such as broken inversion and time-reversal symmetries that affect the details of the Fermi surface in the normal region.

In this work, we performed differential resistance measurements of symmetric and asymmetric four-terminal JJs. In addition to zero-resistance branches corresponding to supercurrent flow between pairs of superconducting terminals, we observed resonant features resembling multiplet Cooper pairings in the differential resistance maps. We observed that the size of the CCC monotonically increased with the increasing gate voltage due to the symmetric Fermi surface of graphene.

We modeled our junctions using a network of coupled RCSJs to elucidate the experimental results. We theoretically investigated the contributions of quasiparticle and pair currents to the total current. Crucially, we found resonant features arising from circuit-network effects that mimic signatures of multiplet pairings. For fixed values of shunt resistance and capacitance, our calculations demonstrated that the multiplet features are insensitive to diffusive, ballistic, or φ_0 -shifted CPRs. Our joint experimental and theoretical study paves the way toward using MTJJs as a materials-agnostic platform for engineering complex superconducting mechanisms involving multiple Cooper pairs.

The experimental data supporting the conclusions of this letter is available on Zenodo [46].

We acknowledge funding from the National Science Foundation (NSF) Innovation and Technology Ecosystems (Grant No. 2040667). F.Z. and N.S. acknowledge support from the University of Chicago. G.J.C. acknowledges support from the ARAP program of the Office of the Secretary of Defense. M.J.G. and M.T.A. acknowledge funding from US ARO Grant No. W911NF-20-2-0151 and the NSF through the University of Illinois at Urbana-Champaign Materials Research Science and Engineering Center DMR-1720633.

- [1] M. Kjaergaard, M. E. Schwartz, J. Braumüller, P. Krantz, J. I.-J. Wang, S. Gustavsson, and W. D. Oliver, Superconducting qubits: Current state of play, Annu. Rev. Condens. Matter Phys. 11, 369 (2020).
- [2] N. P. de Leon, K. M. Itoh, D. Kim, K. K. Mehta, T. E. Northup, H. Paik, B. Palmer, N. Samarth, S. Sangtawesin, and D. Steuerman, Materials challenges and opportunities for quantum computing hardware, Science 372, eabb2823 (2021).
- [3] A. Freyn, B. Douçot, D. Feinberg, and R. Mélin, Production of Nonlocal Quartets and Phase-Sensitive Entanglement in a Superconducting Beam Splitter, Phys. Rev. Lett. 106, 257005 (2011).
- [4] R. de Bruyn Ouboter and A. Omelyanchouk, Multi-terminal squid controlled by the transport current, Phys. B: Condens. Matter 205, 153 (1995).
- [5] M. Amin, A. Omelyanchouk, and A. Zagoskin, Mesoscopic multiterminal josephson structures. I. Effects of nonlocal weak coupling, Low Temp. Phys. 27, 616 (2001).
- [6] M. Amin, A. Omelyanchouk, and A. Zagoskin, Dc squid based on the mesoscopic multiterminal josephson junction, Physica C: Superconductivity 372-376, 178 (2002).
- [7] J. C. Cuevas and H. Pothier, Voltage-induced Shapiro steps in a superconducting multiterminal structure, Phys. Rev. B 75, 174513 (2007).
- [8] B. van Heck, S. Mi, and A. R. Akhmerov, Single fermion manipulation via superconducting phase differences in multiterminal Josephson junctions, Phys. Rev. B 90, 155450 (2014).
- [9] T. Yokoyama and Y. V. Nazarov, Singularities in the Andreev spectrum of a multiterminal Josephson junction, Phys. Rev. B 92, 155437 (2015).

- [10] R.-P. Riwar, M. Houzet, J. S. Meyer, and Y. V. Nazarov, Multi-terminal Josephson junctions as topological matter, Nat. Commun. 7, 11167 (2016).
- [11] E. Eriksson, R.-P. Riwar, M. Houzet, J. S. Meyer, and Y. V. Nazarov, Topological transconductance quantization in a four-terminal Josephson junction, Phys. Rev. B 95, 075417 (2017).
- [12] J. S. Meyer and M. Houzet, Nontrivial Chern Numbers in Three-Terminal Josephson Junctions, Phys. Rev. Lett. 119, 136807 (2017).
- [13] H.-Y. Xie, M. G. Vavilov, and A. Levchenko, Weyl nodes in andreev spectra of multiterminal Josephson junctions: Chern numbers, conductances, and supercurrents, Phys. Rev. B 97, 035443 (2018).
- [14] H.-Y. Xie, M. G. Vavilov, and A. Levchenko, Topological Andreev bands in three-terminal Josephson junctions, Phys. Rev. B 96, 161406 (2017).
- [15] H.-Y. Xie, J. Hasan, and A. Levchenko, Non-abelian monopoles in the multiterminal Josephson effect, Phys. Rev. B 105, L241404 (2022).
- [16] L. P. Gavensky, G. Usaj, and C. A. Balseiro, Topological phase diagram of a three-terminal Josephson junction: From the conventional to the Majorana regime, Phys. Rev. B 100, 014514 (2019).
- [17] H.-Y. Xie and A. Levchenko, Topological supercurrents interaction and fluctuations in the multiterminal Josephson effect, Phys. Rev. B 99, 094519 (2019).
- [18] J. Erdmanis, Á. Lukács, and Y. V. Nazarov, Weyl disks: Theoretical prediction, Phys. Rev. B 98, 241105 (2018).
- [19] E. V. Repin, Y. Chen, and Y. V. Nazarov, Topological properties of multiterminal superconducting nanostructures: Effect of a continuous spectrum, Phys. Rev. B 99, 165414 (2019).

- [20] X.-L. Huang and Y. V. Nazarov, Topology protection—unprotection transition: Example from multiterminal superconducting nanostructures, Phys. Rev. B 100, 085408 (2019).
- [21] E. Strambini, S. D'Ambrosio, F. Vischi, F. Bergeret, Y. V. Nazarov, and F. Giazotto, The ω -squipt as a tool to phase-engineer Josephson topological materials, Nat. Nanotechnol. **11**, 1055 (2016).
- [22] A. W. Draelos, M.-T. Wei, A. Seredinski, H. Li, Y. Mehta, K. Watanabe, T. Taniguchi, I. V. Borzenets, F. Amet, and G. Finkelstein, Supercurrent flow in multiterminal graphene Josephson junctions, Nano Lett. 19, 1039 (2019).
- [23] E. G. Arnault, S. Idris, A. McConnell, L. Zhao, T. F. Larson, K. Watanabe, T. Taniguchi, G. Finkelstein, and F. Amet, Dynamical stabilization of multiplet supercurrents in multiterminal Josephson junctions, Nano Lett. 22, 7073 (2022).
- [24] K.-F. Huang, Y. Ronen, R. Mélin, D. Feinberg, K. Watanabe, T. Taniguchi, and P. Kim, Evidence for 4e charge of cooper quartets in a biased multi-terminal graphene-based Josephson junction, Nat. Commun. 13, 3032 (2022).
- [25] Y. Cohen, Y. Ronen, J.-H. Kang, M. Heiblum, D. Feinberg, R. Mélin, and H. Shtrikman, Nonlocal supercurrent of quartets in a three-terminal Josephson junction, Proc. Natl. Acad. Sci. 115, 6991 (2018).
- [26] N. Pankratova, H. Lee, R. Kuzmin, K. Wickramasinghe, W. Mayer, J. Yuan, M. G. Vavilov, J. Shabani, and V. E. Manucharyan, Multiterminal Josephson Effect, Phys. Rev. X 10, 031051 (2020).
- [27] G. V. Graziano, M. Gupta, M. Pendharkar, J. T. Dong, C. P. Dempsey, C. Palmstrøm, and V. S. Pribiag, Selective control of conductance modes in multi-terminal Josephson junctions, Nat. Commun. 13, 5933 (2022).
- [28] G. V. Graziano, J. S. Lee, M. Pendharkar, C. J. Palmstrøm, and V. S. Pribiag, Transport studies in a gate-tunable three-terminal Josephson junction, Phys. Rev. B **101**, 054510 (2020).
- [29] M. Gupta, G. V. Graziano, M. Pendharkar, J. T. Dong, C. P. Dempsey, C. Palmstrøm, and V. S. Pribiag, Superconducting diode effect in a three-terminal Josephson device, arXiv:2206.08471.
- [30] A. H. Pfeffer, J. E. Duvauchelle, H. Courtois, R. Mélin, D. Feinberg, and F. Lefloch, Subgap structure in the conductance of a three-terminal Josephson junction, Phys. Rev. B 90, 075401 (2014).
- [31] A. Melo, V. Fatemi, and A. Akhmerov, Multiplet supercurrent in Josephson tunneling circuits, SciPost Physics 12, 017 (2022).
- [32] See Supplemental Material at http://link.aps.org/supplemental/ 10.1103/PhysRevB.107.L140503 for additional transport data and RCSJ model parameters.
- [33] J. Xiang, A. Vidan, M. Tinkham, R. M. Westervelt, and C. M. Lieber, Ge/Si nanowire mesoscopic Josephson junctions, Nat. Nanotechnol. 1, 208 (2006).
- [34] L. A. Jauregui, M. Kayyalha, A. Kazakov, I. Miotkowski, L. P. Rokhinson, and Y. P. Chen, Gate-tunable supercurrent and mul-

- tiple Andreev reflections in a superconductor-topological insulator nanoribbon-superconductor hybrid device, Appl. Phys. Lett. **112**, 093105 (2018).
- [35] I. V. Borzenets, F. Amet, C. T. Ke, A. W. Draelos, M. T. Wei, A. Seredinski, K. Watanabe, T. Taniguchi, Y. Bomze, M. Yamamoto, S. Tarucha, and G. Finkelstein, Ballistic Graphene Josephson Junctions from the Short to the Long Junction Regimes, Phys. Rev. Lett. 117, 237002 (2016).
- [36] F. Bergeret and J. Cuevas, The vortex state and Josephson critical current of a diffusive SNS junction, J. Low Temp. Phys. 153, 304 (2008).
- [37] D. McCumber, Effect of ac impedance on dc voltage-current characteristics of superconductor weak-link junctions, J. Appl. Phys. 39, 3113 (1968).
- [38] D. McCumber, Tunneling and weak-link superconductor phenomena having potential device applications, J. Appl. Phys. 39, 2503 (1968).
- [39] R. Jacquet, A. Popoff, K.-I. Imura, J. Rech, T. Jonckheere, L. Raymond, A. Zazunov, and T. Martin, Theory of nonequilibrium noise in general multiterminal superconducting hybrid devices: Application to multiple cooper pair resonances, Phys. Rev. B 102, 064510 (2020).
- [40] T. Jonckheere, J. Rech, T. Martin, B. Douçot, D. Feinberg, and R. Mélin, Multipair dc Josephson resonances in a biased all-superconducting bijunction, Phys. Rev. B 87, 214501 (2013).
- [41] R. Mélin, D. Feinberg, H. Courtois, C. Padurariu, A. Pfeffer, J. E. Duvauchelle, F. Lefloch, T. Jonckheere, J. Rech, T. Martin, and B. Doucot, D.c. Josephson transport by quartets and other Andreev resonances in superconducting bijunctions, J. Phys.: Conf. Ser. 568, 052006 (2014).
- [42] R. Mélin, M. Sotto, D. Feinberg, J.-G. Caputo, and B. Douçot, Gate-tunable zero-frequency current cross correlations of the quartet state in a voltage-biased three-terminal Josephson junction, Phys. Rev. B 93, 115436 (2016).
- [43] M. Alidoust, G. Sewell, and J. Linder, Superconducting phase transistor in diffusive four-terminal ferromagnetic Josephson junctions, Phys. Rev. B 85, 144520 (2012).
- [44] F. Zhang, M. T. Ahari, A. S. Rashid, G. J. de Coster, T. Taniguchi, K. Watanabe, M. J. Gilbert, N. Samarth, and M. Kayyalha, Reconfigurable magnetic-field-free superconducting diode effect in multi-terminal Josephson junctions, arXiv:2301.05081.
- [45] A. Buzdin, Direct Coupling Between Magnetism and Superconducting Current in the Josephson φ_0 Junction, Phys. Rev. Lett. **101**, 107005 (2008).
- [46] F. Zhang, A. S. Rashid, M. T. Ahari, W. Zhang, K. M. Ananthanarayanan, R. Xiao, G. J. de Coster, M. J. Gilbert, N. Samarth, M. Kayyalha, dataset for "Andreev processes in mesoscopic multi-terminal graphene Josephson junctions", 2023, Zenodo, https://doi.org/10.5281/zenodo.7768765.